Modified V-Groove Slot Waveguide for DNA Hybridization Detection

Eman ELDamarawy [1,2], Ahmed M. Heikal [1,3], Salah S. A. Obayya [3*], and Mohamed Farhat O. Hameed [3,4,5*]

[1] Electronic and Electrical Engineering Department, Faculty of Engineering, Mansoura University, 35516, Egypt

[2] Basic Sciences, Higher Future Institute of Engineering and Technology in Mansoura, Mansoura 51, Egypt

[3] Centre for Photonics and Smart Materials, Zewail City of Science and Technology, October Gardens
6th of October City, Giza 12578, Egypt
sobayya@zewailcity.edu.eg*

[4] Nanotechnology and Nanoelectronics Program, Zewail City of Science and Technology, October Gardens
6th of October City, Giza 12578, Egypt
mfarahat@zewailcity.edu.eg*

[5] Mathematics and Engineering Physics Department, Faculty of Engineering, Mansoura University
Mansoura 35516, Egypt

***Abstract* —** Highly sensitive slot waveguides are introduced and studied for DNA hybridization detection. In this investigation, two different configurations based on V-groove silicon on insulator (SOI) waveguides are analyzed using full vectorial finite element method. The suggested designs rely on improving the light confinement through the slot region at an operating wavelength of 1.55 μm. The power confinement, power density (*PD*), and effective index of the supported modes are studied for the conventional rectangular slot waveguide and proposed designs. Further, the effect of adding a plasmonic layer to the reported slot waveguides is implemented. It has been shown that the plasmonic layer increases the light confinement in the slot region with high potential for DNA hybridization detection with good confinement through the slot region.

***Index Terms* —** DNA biosensors, DNA hybridization, plasmonics, slot waveguides, V-groove.

I. INTRODUCTION

Biosensors have many applications in our daily life such as food analysis [1], biomolecules study [2], drug development [3], crime detection [4] and medical diagnosis [5]. The biomedical sensor can integrate the biological elements with the physiochemical transducer to produce a signal that mimics any small change in the properties of the biological element. There are many kinds of biosensors such as electrochemical biosensors, optical biosensors and piezoelectric biosensors. However, optical biosensors [6] could enable direct and real-time detection of many biological and chemical substances [7]. Further, high sensitivity, compact size, remote sensing and cost-effectiveness could be realized using optical biosensors. The optical detection relies on the interaction of the optical field with a bio-recognition element. Additionally, optical biosensors are based on label free or label-based techniques. The detected signal in label free biosensor is generated by the interaction of the analyte with the transducer. However, label and the optical signal generated by a colorimetric are needed in label based biosensors.

There are many platforms that can be used for optical sensing applications such as photonic crystal [8] and silicon on insulator (SOI) [9]. In this context, SOI microring cavity was proposed for protein concentration detection [10]. Additionally, a label-free integrated biosensor based on Si_3N_4/SiO_2 slot waveguide has been used to detect the Bouie serum albumin (BSA) and anti-BSA molecular [11]. Moreover, SOI ring resonator based biosensor has been presented for protein sensing [12]. However, most optical waveguide biosensors are based on light confinement in the denser medium with limited interaction with the sensing medium. The slot waveguide has an advantage of light confinement in the slot low index region. This will improve the interaction between the light and the sensing medium with enhanced sensor sensitivity.

The DNA hybridization is a molecular biology technique that measures the degree of genetic similarity

Submitted On: December 25, 2019
Accepted On: May 5, 2020

between pools of DNA sequences. It is usually used to determine the genetic distance between two organisms. Through the DNA hybridization process, the single stranded DNA (ssDNA) is transformed into double stranded DNA (dsDNA) when the two complement ssDNA sequences are merged together. DNA hybridization detection [13] is very helpful for several applications such as genetic detection, [14], medicinal bio-engineering [15] and clinical diagnostics [16]. The DNA analysis has been performed using different techniques such as restriction fragment length polymorphism [17], short tandem repeats [18], mitochondria analysis [19] and polymerase chain reaction [20]. The electrochemical sensor [21] is the most popular DNA detection technique [22] with low cost, high sensitivity and high selectivity [23]. There are also several nanomaterials that have been used in DNA biosensors like metallic nanoparticles [24], carbon nanomaterials [25] semiconductor metal oxide [26] and two dimensional transition metal sulfide [27]. Optical biosensors have been recently used for DNA hybridization detection. Most of the DNA biosensors rely on dielectric materials with different configurations [28] such as Mach-Zehnder interferometer [29]. Additionally, the light can be strongly confined in the slot waveguide by using surface plasmon polaritons (SPPs) [30]. The SPPs are resulted from the light interaction with the surface free electrons of the metal. Gold and silver [31] are the widely used metals in sensing applications due to their high conductivity with low Ohmic losses. The silver has high detection accuracy [32] with low chemical stability owing to its oxidation problem. Therefore, it is difficult to obtain reproducible results and hence the silver based sensor is not reliable for practical applications [33].

In this paper, the potential of using V-groove SOI based slot waveguides is introduced for DNA hybridization detection. The rectangular slot biosensor has been previously reported [7] for DNA hybridization detection. In order to increase the confinement of the field in the slot region, V-groove slot types are presented in this work. The V-groove shape can be achieved by etching the edges with an angle θ. This angle has a significant effect on the light confinement through the slot region. Therefore, a modified V-groove design is suggested to simplify the fabrication process and achieve good confinement with a good potential for detecting DNA hybridization. The possibility of adding plasmonic material to the reported designs is also implemented. It is found that the field confinement through the slot region and the power density (*PD*) in the DNA layers are improved significantly using the plasmonic material. Therefore, the DNA hybridization detection could be achieved effectively.

II. DESIGN CONSIDERATIONS

Figure 1 shows schematic diagrams of the conventional rectangular slot waveguide, V-groove and modified V-groove structures. The conventional structure consists of two silicon waveguides with width W, length H and refractive index (RI) of 3.476 [7] at a wavelength of 1550 nm. The silicon nanowires are separated by a distance of SW and are placed over SiO_2 layer with RI = 1.444 as shown in $Fig.$ 1 (a). Further, the silicon waveguides are covered by a linker layer (silanes) with RI and thickness t_{Linker} of 1.42 and 1 nm, respectively [34]. Then, single-stranded DNA (ssDNA) (probe layer) of thickness t_{DNA} = 8 nm and RI= 1.456 is used. The double-stranded DNA (dsDNA) with RI=1.53 [35] will be formed due to the hybridization process with fixed layer thickness. Initially, the silicon waveguides have H = 320 nm, W = 180 nm and SW = 40 nm surrounded by an analyte H_2O with refractive index of 1.31. *Figure* 1 (b) illustrates the V-groove slot waveguide with an angle θ and fixed height (H) similar to the rectangular waveguide. In the modified V-groove, the parameter g shown in $Fig.$ 1 (c) stands for the minimal bottom gap distance between the two layers of the DNA which is taken as g=22 nm.

III. NUMERCAL METHOD

From Maxwell's equations, the vector wave equation of the magnetic field will be as follows:

$$\nabla \times \left(\varepsilon_r^{-1}\nabla \times \vec{H}\right) - \omega^2 \mu_0 \vec{H} = 0, \qquad (1)$$

where ω is the angular frequency, μ_0 is the free space permeability and $\varepsilon = \varepsilon_0\varepsilon_r$ is the permittivity of the waveguide material, ε_0 is the free space permittivity and ε_r is relative permittivity of the composing material. The cross section of the waveguide structure is discretized using vector finite element method [36]. The following eigenvalue equation can be derived:

$$[K]\{H\} - \beta^2[M]\{H\} = \{0\}, \qquad (2)$$

where [K] and [M] are the global stiffness and mass matrices, {H} is the global magnetic field vector, {0} is the null vector and $\boldsymbol{\beta}$ is the propagation constant. The eigenvalue equation can be solved to obtain the eigenvector H, and the corresponding eigenvalue $\boldsymbol{\beta}$. Then, the effectively index of the supported mode is calculated from $n_{eff}=\boldsymbol{\beta}/K$ where K is the free space wave number.

The full vectorial finite element method (FVFEM) via Comsol Multiphysics software package [37] is utilized to study the optical characteristics of the suggested designs. In this study, total number of elements of 55181 is used with perfect matched layer boundary conditions and minimum element size of 0.04 nm.

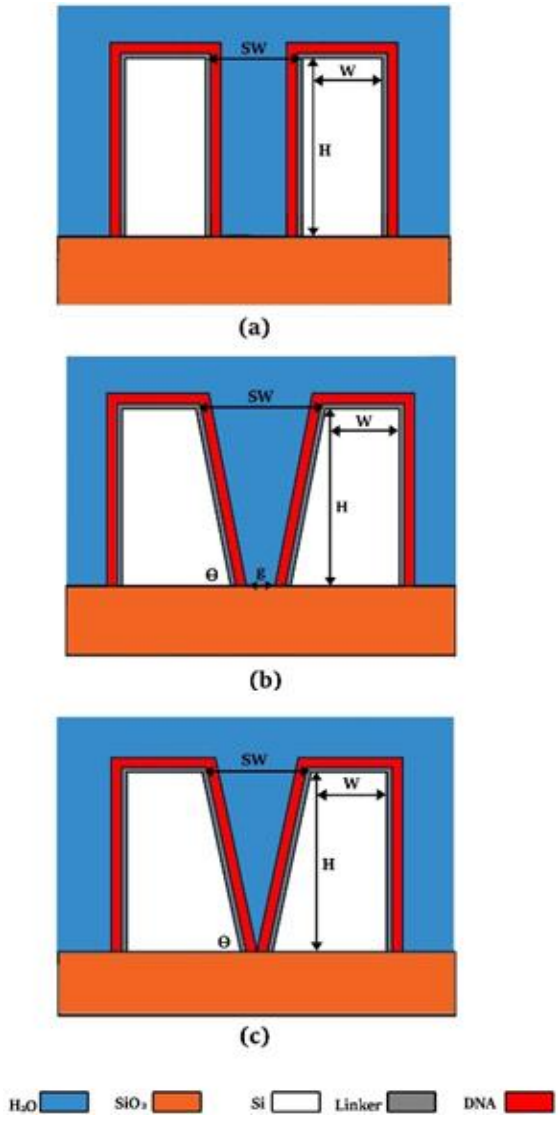

Fig. 1. Schematic diagrams of the: (a) rectangular waveguide, (b) modified V-groove SOI, and (c) V-groove SOI for DNA hybridization detection.

IV. RESULTS AND DISCUSSION

Figure 2 illustrates the E_x field component of the supported transverse electric (TE) mode of the rectangular, V-groove and modified V-groove designs at λ=1.55 μm. Further, the power flow P_z in the z-direction through the studied designs is shown in $Fig.$ 2. It is revealed from this figure that high field confinement is achieved in the low index region due to the high index contrast between the analyte and the silicon nanowires. The highest field confinement is achieved using the V-groove based designs. Therefore, it is expected that the V-groove based biosensors can achieve high sensitivity for DNA hybridization detection. In this work, the power over the DNA region is normalized to the total power through the studied waveguide as shown in equation (3). The power density (*PD*) can be obtained from the normalized power confinement divided by the area of the DNA layer as represented in equation (4). The highest *PD* through the proposed designs is achieved by the V-groove structure which confirms the field confinement shown in $Fig.$ 2.

Normalized power confinement %=

$$\frac{Power\ over\ the\ DNA\ region}{Total\ power\ over\ the\ waveguide}\times 100\%, \quad (3)$$

$$\text{Power density}=\frac{Normalized\ power\ confinement\ \%}{Area\ of\ the\ DNA\ reion}. \quad (4)$$

The main purpose of these designs is to improve the light confinement in the slot region. Therefore, the DNA hybridization detection capability can be increased. Consequently, the geometrical parameters of the V-groove and modified V-groove structures will be studied. First, the effect of the silicon waveguide width W is investigated. In this study, the silicon waveguide height is taken as 320 nm, θ = 77, and g = 22 nm. Figures 3 (a) and (c) show the effective index n_{eff} and δn_{eff} dependence of the quasi-TE mode for the ssDNA and dsDNA cases on the silicon waveguide width W for the V-groove and modified V-groove, respectively. Additionally, Figs. 3 (b), and (d) illustrate the dependence of the *PD* on the width (W). The change in the effective index δn_{eff} of the supported mode can be defined as $\delta n_{eff}= n_{eff-dsDNA} - n_{eff-ssDNA}$. The δn_{eff} is obtained by simulating the proposed design with ssDNA layer (n=1.456) above the linker layer. Then, the ssDNA is replaced by dsDNA with n=1.53. It may be seen that the maximum δn_{eff} is obtained at W = 210 nm of the V-groove as shown in Fig. 3 (a). Further, maximum PD also occurs at $W = 210\ nm$ as shown in Fig. 3 (b) due to the well confinement of the mode in the slot region. Therefore, a good light interaction with the analyte in the slot region can be achieved with expected high sensor sensitivity. It is worth noting that the ssDNA has a smaller refractive index than that of the dsDNA. Consequently, the PD through the ssDNA case is greater than that of the dsDNA as revealed from Fig. 3. It is also evident from Figs. 3 (c) and (d) that the maximum δn_{eff} and PD of the modified V-groove are achieved at W = 200 nm and 170 nm, respectively. Therefore, $W = 170\ nm$ is chosen for the next simulations of the modified V-grove design to have good light interaction with the studied analyte.

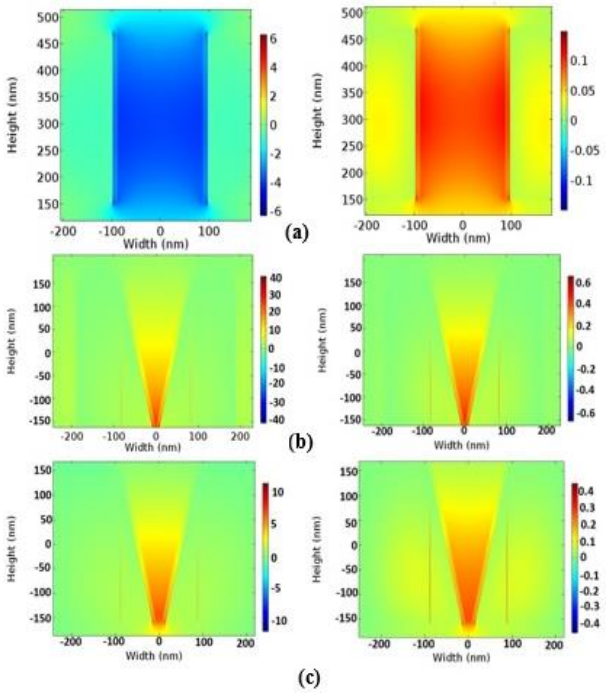

Fig. 2. The E_x field component and the power flow P_z of the quasi-TE mode at λ = 1.55 µm of the: (a) rectangular waveguide, (b) V-groove, and (c) and modified V-groove structures.

The effect of the waveguide height H is next studied at $W = 210\ nm$ for the V-groove design and at $W = 170\ nm$ for the modified V-groove. Figures 4 (a) and (b) show the dependence of the PD through the $ssDNA$ and $dsDNA$ layers on the silicon waveguide height of the V-groove and modified V-groove designs. It is evident from $Fig.$ 4 that the maximum PD is obtained at H = 220 nm of the V-groove and modified V-groove with high field confinement through the slot region. It should be noted that a height of 220 nm is chosen according to the well-known standard height of the SOI waveguide to simplify the fabrication process. Additionally, H >220 nm is studied to ensure the etching feasibility of the suggested design.

The effect of the angle θ is then studied through $Figs.$ 5. (a) and (b). In this investigation, W = 210 nm and H = 220 nm for the V-groove design. However, the modified V-groove design has W = 170 nm, H =220 nm and g = 12 nm. It may be seen that an angle $\theta = 86^{o}$ results in maximum PD for both the V-groove and modified V-groove which could achieve high DNA hybridization detection. $Figure$ 5 (c) shows the effect of the distance g of the modified V-groove at $\theta = 86^{o}$ where maximum PD occurs at g= 12 nm. If the gap is decreased to 5 nm, the PD will be significantly decreased to 2.26 for ssDNA and 2.13 for dsDNA cases.

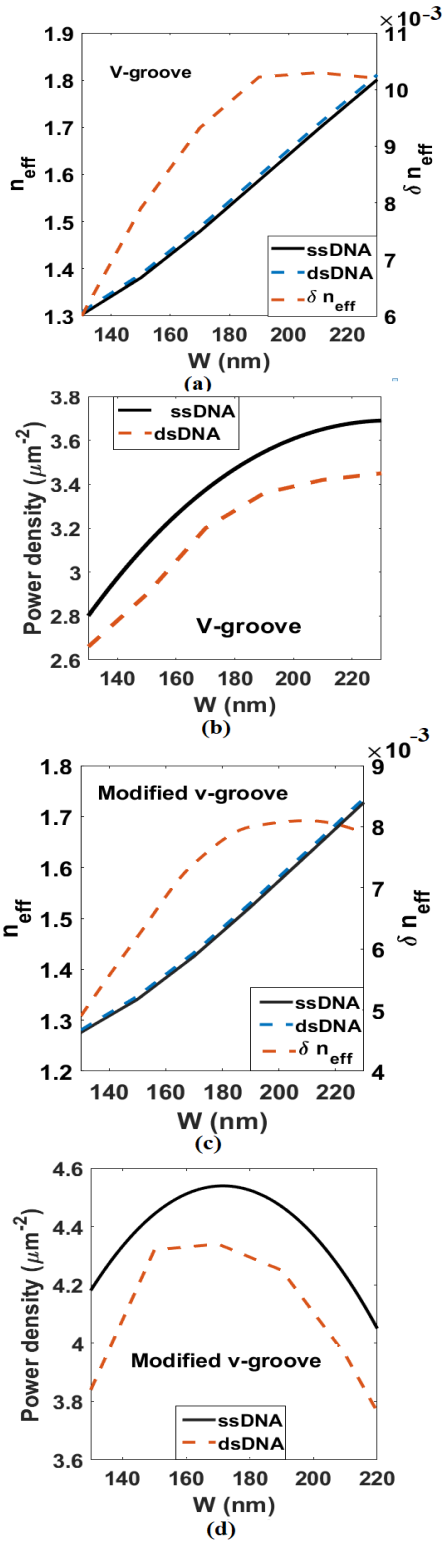

Fig. 3. Dependence of the n_{eff}, δn_{eff} and PD of the quasi-TE mode on the width (W) of the: (a), (b) V-groove, and (c), (d) modified V-groove designs using $ssDNA$ and $dsDNA$ layers.

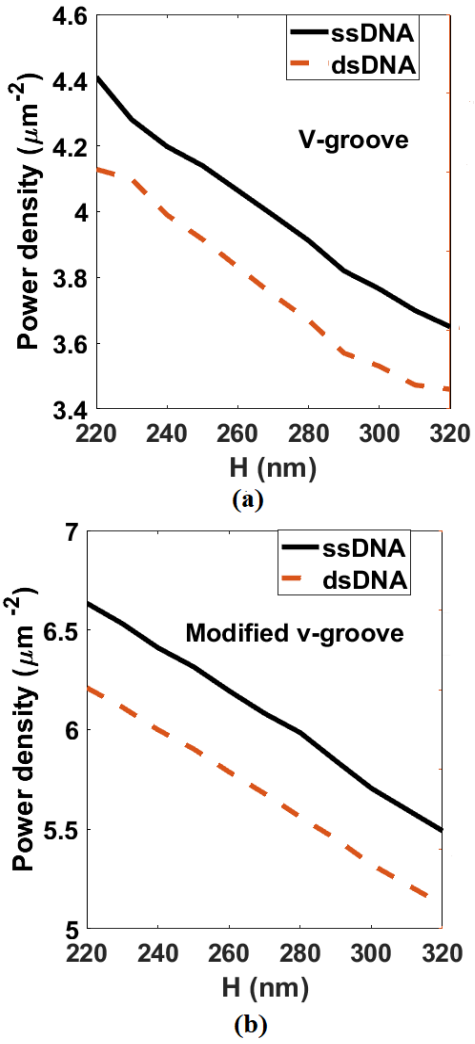

Fig. 4. Dependence of the *PD* of the quasi-TE mode with $ssDNA$ and $dsDNA$ layers on the height (H) of the: (a) V-groove and (b) modified V-groove designs using ssDNA and dsDNA layers.

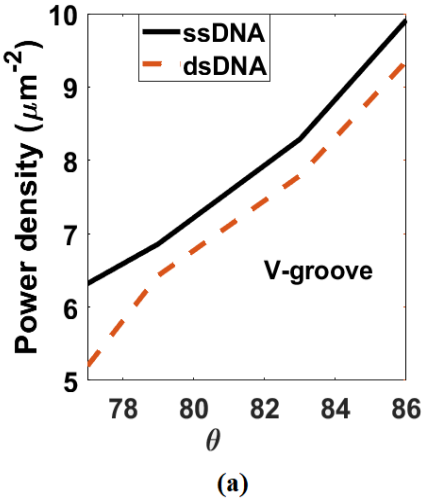

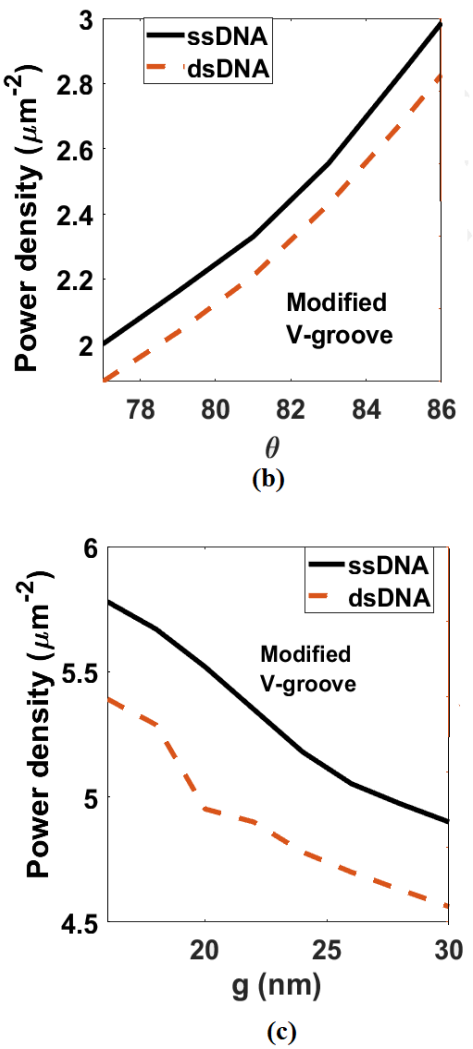

Fig. 5. Dependence of the *PD* of the quasi-TE mode of the proposed designs on the angle θ for the: (a) V-groove, and (b) modified V-groove using ssDNA and dsDNA layers. Fig. 5 (c) illustrates the *PD* of the quasi-TE mode variation with the distance (g) nm of the modified V-groove structure.

Next, a gold layer is added above the SiO_2 material to improve the light confinement in the slot region as shown in Fig. 6. Then, the DNA hybridization detection capability could be improved. The gold layer with thickness (t) has the following relative permittivity [38,39]:

$$\varepsilon_{Au}(\omega) = \varepsilon_{\infty} - \frac{\omega_p^2}{\omega(\omega + i\omega_\tau)}, \tag{5}$$

where ε_∞ = 9.75, ω_p = 1.36 × 10^{16} (rad/sec) and ω_τ = 1.45 × 10^{14} (rad/sec). In this investigation, the V-groove design has H = 220 nm, t (gold thickness) = 50 nm and θ = 86°. The *PD* dependence on the silicon width is first studied as shown in $Fig.$ 7. The figure shows that the V-

groove has high light confinement at W = 240 nm which differs from the geometrical parameters of the V-groove without plasmonic material. *Figure* 7 (b) shows that the appropriate width for the modified V-groove is equal to W = 250 nm with maximum *PD*.

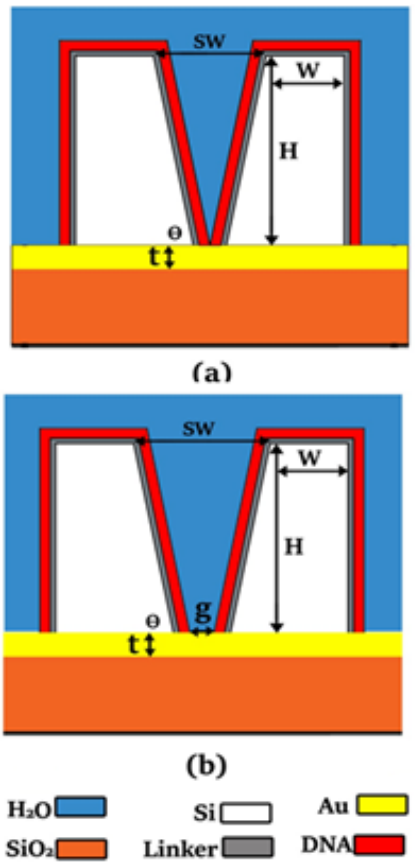

Fig. 6. Schematic diagram of the plasmonic: (a) V-groove and (b) modified V-groove designs.

The effect of the angle θ will be studied for the two suggested designs; V-groove and modified V-groove. As θ increases, the light confinement through the slot region and the *PD* of the supported quasi TE mode are increased for the V-groove and modified V-groove designs as shown in $Fig.9$. The highest *PD* of the V-groove and modified V-groove designs are obtained at θ =80° with high field confinement in the slot region. It may be also seen that the ssDNA has higher *PD* than that occurs for the dsDNA case. This is because of the smaller RI of the ssDNA than the dsDNA.

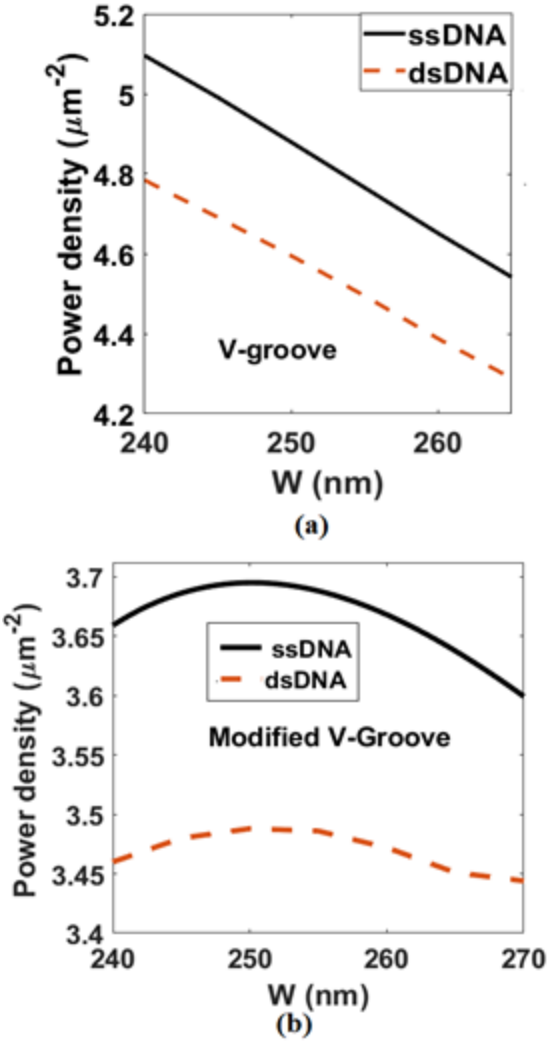

Fig. 7. Dependence of the *PD* of the quasi-TE mode of the plasmonic designs with $ssDNA$ and $dsDNA$ layers and gold layer with t=50nm on the width (W) of the: (a) V-groove and (b) modified V-groove designs.

The impact of the waveguide height H is next studied at W = 240 nm for the plasmonic V-groove design. For the modified V-groove design, $W = 250\ nm$ is taken for this study. The dependence of the *PD* though the plasmonic designs with $ssDNA$ and $dsDNA$ layers on the silicon waveguide height of the V-Groove and modified V-groove designs is shown in *Fig.* 8 at t=50 nm. *Figure* 8 (a) shows that the highest *PD* occurs at H = 220 nm of the V-groove and at $H = 240\ nm$ for the

modified V-groove with high field confinement through the slot region.

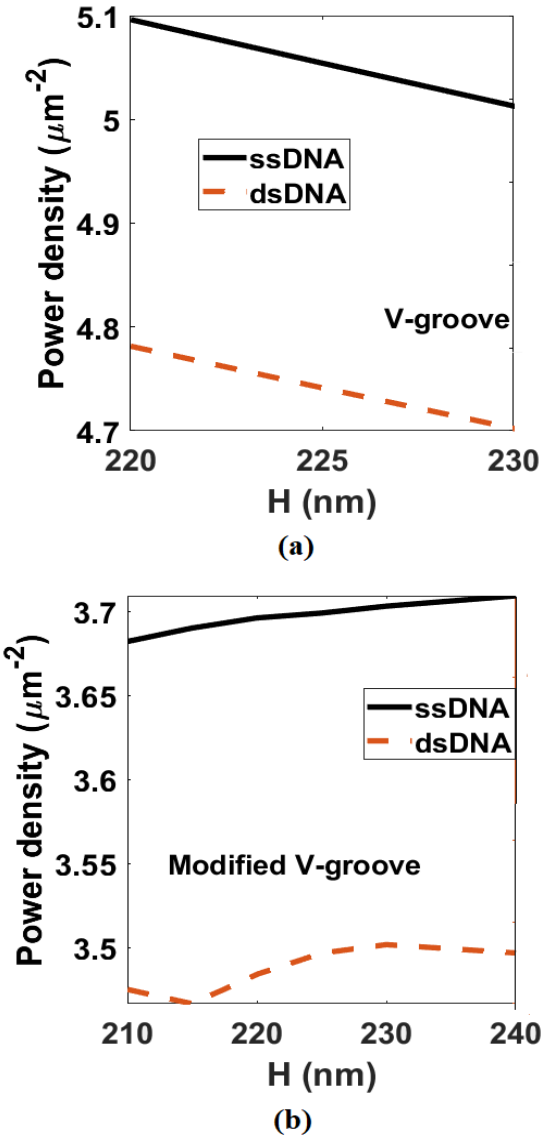

Fig. 8. Variation of the *PD* at t= 50nm with width (H) and its *PD* of the: (a) V-groove and (b) modified V-groove designs with ssDNA and dsDNA layers.

The effect of the distance $g\ (nm)$ in the modified V-groove is also introduced at $t = 50\ nm$ as shown in $Fig.10$. It can be seen that the maximum *PD* occurs at $g = 50\ nm$ for high filed confinement through the slot region. Finally, the thickness (t) of the plasmonic layer is studied to enhance the field confinement in the slot region. $Figure\ 11$ shows that the best thickness for both V-groove and modified V-groove will be obtained at $t = 50\ nm$ which will be appropriate for the fabrication process. The optimum geometrical parameters of the plasmonic V-groove designs are summarized in Table 1 to obtain maximum *PD* and maximum confinement.

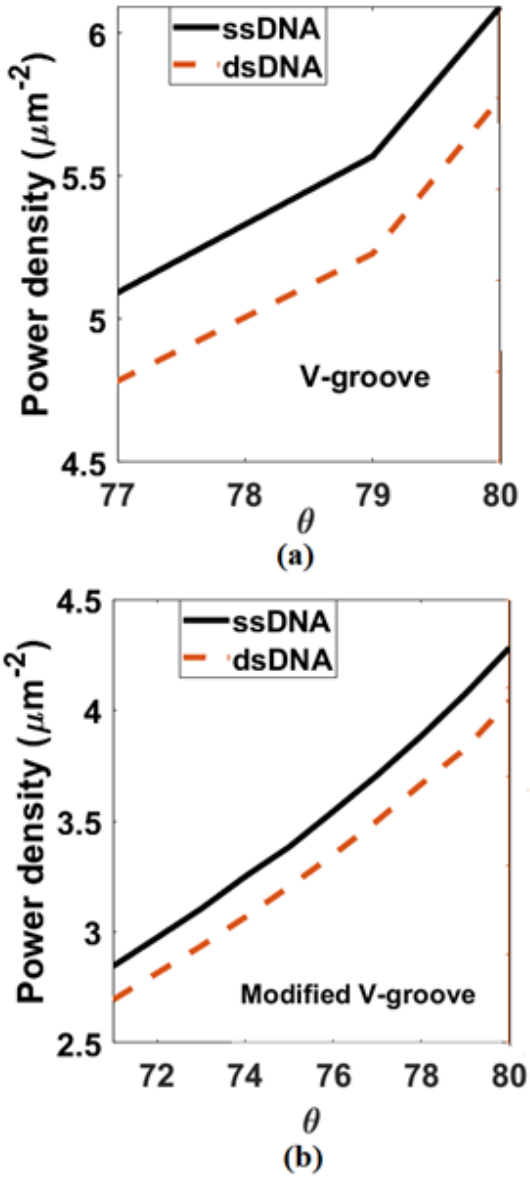

Fig. 9. Variation of the *PD* at t= 50 nm with an angle (θ) and its *PD* for the: (a) V-groove and (b) modified V-groove designs with ssDNA and dsDNA layers.

The fabrication of the suggested designs can be achieved using the standard SOI fabrication technology [40]. In this context, conventional rectangular slot waveguide is previously implemented in [41]. Additionally, the fabrication of V-groove structure has been reported in different applications [42, 43, 44]. Further, the deposition of plasmonic materials over SOI waveguides can be realized by atomic layer deposition [45]. Therefore, the suggested designs can be realized using the current technology.

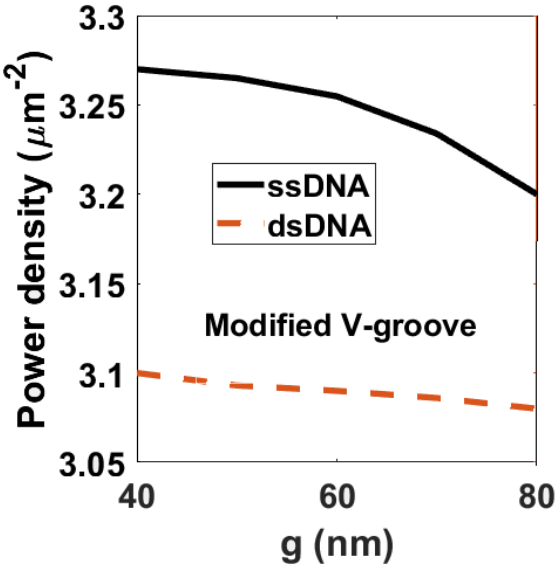

Fig. 10. Variation of the *PD* at $t = 50\,nm$ with the distance $(g)nm$ for modified v-groove design with ssDNA and dsDNA layers.

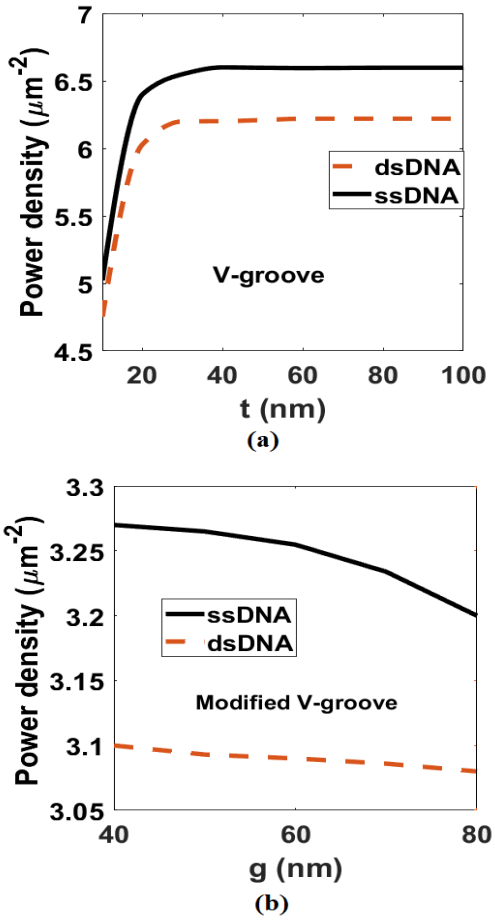

Fig. 11. Variation of the *PD* with the gold layer thickness (t) nm for the: (a) V-groove and (b) modified V-groove designs with ssDNA and dsDNA layers.

Table 1: The optimized parameters of the plasmonic V-groove and modified V-groove SOI structures

Parameter	V-groove	Modified V-groove
t	50 nm	50 nm
W	240 nm	250 nm
H	220 nm	240 nm
θ	80°	80°
g	-	40 nm

V. CONCLUSION

Modified slot waveguides are suggested and optimized for DNA hybridization detection capabilities. This is due to the dependence of the refractive index of the DNA layer on the hybridization process. In this investigation, three designs are studied including rectangular waveguide, V-groove and modified V-groove structure based on SOI platform. It is found that the power confinement and *PD* of the V-groove slot waveguide is higher than those of the other designs. However, the modified V-design is easier for real implementation. Further, the addition of plasmonic layer increases the light confinement in the low index region with high potential for DNA hybridization detection with good confinement through the slot region.

REFERENCES

[1] A. Agrawal, R. A. Tripp, L. J. Anderson, and S. Nie, "Real-time detection of virus particles and viral protein expression with two-color nanoparticle probes," *J. Virol.*, vol. 79, no. 13, pp. 8625-8628, 2005.

[2] K. Kneipp, *et al.*, "Single molecule detection using surface-enhanced Raman scattering (SERS),"

Phys. Rev. Lett., vol. 78, no. 9, p. 1667, 1997.

[3] M. D. Hämäläinen, *et al.*, "Characterization of a set of HIV-1 protease inhibitors using binding kinetics data from a biosensor-based screen," *J. Biomol. Screen.*, vol. 5, no. 5, pp. 353-359, 2000.

[4] S. Sumriddetchkajorn and A. Somboonkaew, "Thermal analyzer enables improved lie detection in criminal-suspect interrogations," *SPIE Newsroom Def. Secur.*, 2011.

[5] L. Heinemann and G. Schmelzeisen-Redeker, "Non-invasive continuous glucose monitoring in Type I diabetic patients with optical glucose sensors," *Diabetologia*, vol. 41, no. 7, pp. 848-854, 1998.

[6] M. F. O. Hameed, Y. K. A. Alrayk, A. A. Shaalan, W. S. El Deeb, and S. S. A. Obayya, "Design of highly sensitive multichannel bimetallic photonic crystal fiber biosensor," *J. Nanophotonics*, vol. 10, no. 4, 2016 .

[7] T. Dar, J. Homola, B. M. A. Rahman, and M. Rajarajan, "Label-free slot-waveguide biosensor for the detection of DNA hybridization," *Appl. Opt.*, vol. 51, no. 34, pp. 8195-8202, 2012.

[8] N. F. F. Areed, M. F. O. Hameed, and S. S. A. Obayya, "Highly sensitive face-shaped label-free photonic crystal refractometer for glucose concentration monitoring," *Opt. Quantum Electron.*, vol. 49, no. 1, 2017.

[9] M. F. O. Hameed, A. S. Saadeldin, E. M. A. Elkaramany, and S. S. A. Obayya, "Label-free highly sensitive hybrid plasmonic biosensor for the detection of DNA hybridization," *J. Light. Technol.*, vol. 35, no. 22, pp. 4851-4858, 2017.

[10] K. De Vos, I. Bartolozzi, E. Schacht, P. Bienstman, and R. Baets, "Silicon-on-Insulator microring resonator for sensitive and label-free biosensing," *Opt. Express*, vol. 15, no. 12, pp. 7610-7615, 2007.

[11] C. A. Barrios, *et al.*, "Label-free optical biosensing with slot-waveguides," *Opt. Lett.*, vol. 33, no. 7, pp. 708-710, 2008.

[12] T. Claes, J. G. Molera, K. De Vos, E. Schacht, R. Baets, and P. Bienstman, "Label-free biosensing with a slot-waveguide-based ring resonator in silicon on insulator," *IEEE Photonics J.*, vol. 1, no. 3, pp. 197-204, 2009.

[13] J. Guo, J. Wang, J. Zhao, Z. Guo, and Y. Zhang, "Ultrasensitive multiplexed immunoassay for tumor biomarkers based on DNA hybridization chain reaction amplifying signal," *ACS Appl. Mater. Interfaces*, vol. 8, no. 11, pp. 6898-6904, 2016.

[14] Z. Cheglakov, T. M. Cronin, C. He, and Y. Weizmann, "Live cell microRNA imaging using cascade hybridization reaction," *J. Am. Chem. Soc.*, vol. 137, no. 19, pp. 6116-6119, 2015.

[15] S. X. Chen and G. Seelig, "An engineered kinetic amplification mechanism for single nucleotide variant discrimination by DNA hybridization probes," *J. Am. Chem. Soc.*, vol. 138, no. 15, pp. 5076-5086, 2016.

[16] N. S. Gabr, A. K. Ahmed, U. S. Belal, R. A. M. Abd Rabou, R. F. Ahmed, and E. H. Abdel-Hafeez, "Molecular characterization of Cryptosporidium isolates from humans by nested polymerise chain reaction-restriction fragment length polymorphism (nPCR-RFLP) analysis in Egypt," *Trop. Biomed.*, vol. 36, no. 1, pp. 1-10, 2019.

[17] R. Yano, O. Shimoda, T. Okitsu, M. Sakurada, and Y. Ueno, "Development of a modified p-dimethylaminocinnamaldehyde solution for touch DNA analysis and its application to STR analysis," *Forensic Sci. Int. Genet.*, vol. 38, pp. 86-92, 2019.

[18] T. Devièse, *et al.*, "Compound-specific radiocarbon dating and mitochondrial DNA analysis of the Pleistocene hominin from Salkhit Mongolia," *Nat. Commun.*, vol. 10, no. 1, p. 274, 2019.

[19] E. T. Lagally, C. A. Emrich, and R. A. Mathies, "Fully integrated PCR-capillary electrophoresis microsystem for DNA analysis," *Lab Chip*, vol. 1, no. 2, pp. 102-107, 2001.

[20] S. Z. Mousavisani, J. B. Raoof, R. Ojani, and Z. Bagheryan, "An impedimetric biosensor for DNA damage detection and study of the protective effect of deferoxamine against DNA damage," *Bioelectrochemistry*, vol. 122, pp. 142-148, 2018.

[21] H. Gao, M. Sun, C. Lin, and S. Wang, "Electrochemical DNA biosensor based on graphene and TiO2 nanorods composite film for the detection of transgenic soybean gene sequence of MON89788," *Electroanalysis*, vol. 24, no. 12, pp. 2283-2290, 2012.

[22] A. A. Ensafi, N. Kazemnadi, M. Amini, and B. Rezaei, "Impedimetric DNA-biosensor for the study of dopamine induces DNA damage and investigation of inhibitory and repair effects of some antioxidants," *Bioelectrochemistry*, vol. 104, pp. 71-78, 2015.

[23] M. Y. Azab, M. F. O. Hameed, A. M. Nasr, and S. S. A. Obayya, "Label free detection for DNA hybridization using surface plasmon photonic crystal fiber biosensor," *Opt. Quantum Electron.*, vol. 50, no. 2, 2018.

[24] M. Fojta, A. Daňhel, L. Havran, and V. Vyskočil, "Recent progress in electrochemical sensors and assays for DNA damage and repair," *TrAC Trends Anal. Chem.*, vol. 79, pp. 160-167, 2016.

[25] H. Huang, W. Bai, C. Dong, R. Guo, and Z. Liu, "An ultrasensitive electrochemical DNA biosensor based on graphene/Au nanorod/polythionine for human papillomavirus DNA detection," *Biosens. Bioelectron.*, vol. 68, pp. 442-446, 2015.

[26] M. R. Saidur, A. R. A. Aziz, and W. J. Basirun, "Recent advances in DNA-based electrochemical

biosensors for heavy metal ion detection: A review," *Biosens. Bioelectron.*, vol. 90, pp. 125-139, 2017.

[27] J. Lee, M. Morita, K. Takemura, and E. Y. Park, "A multi-functional gold/iron-oxide nanoparticle-CNT hybrid nanomaterial as virus DNA sensing platform," *Biosens. Bioelectron.*, vol. 102, pp. 425-431, 2018.

[28] C. Viphavakit, M. Komodromos, C. Themistos, W. S. Mohammed, K. Kalli, and B. M. A. Rahman, "Optimization of a horizontal slot waveguide biosensor to detect DNA hybridization," *Appl. Opt.*, vol. 54, no. 15, pp. 4881-4888, 2015.

[29] S. A. Maier, "Plasmonics: Metal nanostructures for subwavelength photonic devices," *IEEE J. Sel. Top. quantum Electron.*, vol. 12, no. 6, pp. 1214-1220, 2006.

[30] M. Y. Azab, M. F. O. Hameed, and S. S. A. Obayya, "Multi-functional optical sensor based on plasmonic photonic liquid crystal fibers," *Opt. Quantum Electron.*, vol. 49, no. 2, 2017.

[31] K. A. Willets and R. P. Van Duyne, "Localized surface plasmon resonance spectroscopy and sensing," *Annu. Rev. Phys. Chem.*, vol. 58, pp. 267-297, 2007.

[32] K. Q. Le, J. Bai, Q. M. Ngo, and P.-Y. Chen, "Fabrication and numerical characterization of infrared metamaterial absorbers for refractometric biosensors," *J. Electron. Mater.*, vol. 46, no. 1, pp. 668-676, 2017.

[33] E. L. S. Wong and J. J. Gooding, "Charge transfer through DNA: a selective electrochemical DNA biosensor," *Anal. Chem.*, vol. 78, no. 7, pp. 2138-2144, 2006.

[34] M. D. Malinsky, K. L. Kelly, G. C. Schatz, and R. P. Van Duyne, "Chain length dependence and sensing capabilities of the localized surface plasmon resonance of silver nanoparticles chemically modified with alkanethiol self-assembled monolayers," *J. Am. Chem. Soc.*, vol. 123, no. 7, pp. 1471-1482, 2001.

[35] X. Li *et al.*, "Sensitive label-free and compact biosensor based on concentric silicon-on-insulator microring resonators," *Appl. Opt.*, vol. 48, no. 25, pp. F90-F94, 2009.

[36] S. S. A. Obayya, B. M. A. Rahman, and H. A. El-Mikati, "New full-vectorial numerically efficient propagation algorithm based on the finite element method," *J. Light. Technol.*, vol. 18, no. 3, pp. 409-415, 2000.

[37] C. Multiphysics, "Introduction to COMSOL Multiphysics®," *COMSOL Multiphysics, Burlington, MA*, accessed Feb., vol. 9, p. 2018, 1998.

[38] A. M. Heikal, M. F. O. Hameed, and S. S. A. Obayya, "Improved trenched channel plasmonic waveguide," *J. Light. Technol.*, vol. 31, no. 13, pp. 2184-2191, 2013.

[39] S. Obayya, M. F. O. Hameed, and N. F. F. Areed, *Computational Liquid Crystal Photonics: Fundamentals, Modelling and Applications*. John Wiley & Sons, 2016.

[40] G. K. Celler and S. Cristoloveanu, "Frontiers of silicon-on-insulator," *J. Appl. Phys.*, vol. 93, no. 9, pp. 4955-4978, 2003

[41] P. Steglich, C. Villringer, S. Pulwer, M. Casalboni, and S. Schrader, "Design optimization of silicon-on-insulator slot-waveguides for electro-optical modulators and biosensors," in *Photoptics 2015*, Springer, pp. 173-187, 2016.

[42] A. d'Alessandro, B. Bellini, D. Donisi, R. Beccherelli, and R. Asquini, "Nematic liquid crystal optical channel waveguides on silicon," *IEEE J. Quantum Electron.*, vol. 42, no. 10, pp. 1084-1090, 2006.

[43] http://www.o-eland.com/passive/FiberArray/vgroove.htm

[44] H.-L. Hsiao, *et al.*, "Compact and passive-alignment 4-channel× 2.5-Gbps optical interconnect modules based on silicon optical benches with 45 micro-reflectors," *Opt. Express*, vol. 17, no. 26, pp. 24250-24260, 2009.

[45] S.-B. Kang, Y. Chae, C. Park, and S. Lee, "Method for forming metal layer using atomic layer deposition." *Google Patents*, Jan. 16, 2001.